

where $X_1(t), \dots, X_n(t)$ are n independent, identically distributed, homogeneous, real valued Gaussian random fields of dimension N with zero mean and unit variance.

Theorem 3.5 of [5] provides the asymptotic result

$$E(M_u^+(U, C)) = \frac{\lambda(C) \det(\Lambda)^{\frac{1}{2}} u^{\frac{1}{2}(n-N)} \exp\left(-\frac{u}{2}\right)}{(2\pi)^{\frac{N}{2}} 2^{\frac{1}{2}(n-2)} \Gamma\left(\frac{n}{2}\right)} \times u^{N-1} \left\{ 1 + O\left(u^{-\frac{1}{2}}\right) \right\} \quad (5)$$

where the expectation of $M_u^+(U, C)$ gives the mean number of maxima greater than u , $\lambda(C)$ is the measure (area or volume) of region C , and Λ is a matrix of second moments of the spectrum of the Gaussian field.

We define the envelope as the square root of the χ^2 field. The false alarm curve may be obtained using the approach described in [2]; we let $n = 2$ in eqn. 6 and obtain the false alarm curve for the χ^2 field as

$$\text{pfa}(u) = 1 - \left(1 - u^{\frac{N}{2}} \exp\left(-\frac{u}{2}\right) \right)^{\frac{V_N \sqrt{\det \Lambda}}{(2\pi)^{N/2}}} \quad (6)$$

where V_N corresponds to the 'volume' of the support of the random field.

The false alarm curve for the envelope may be obtained by replacing u with x^2 giving

$$\text{pfa}(x, N) = 1 - \left(1 - x^N \exp\left(-\frac{x^2}{2}\right) \right)^{\frac{V_N \sqrt{\det \Lambda}}{(2\pi)^{N/2}}} \quad (7)$$

Eqn. 3 may be recovered by letting $N = 1$.

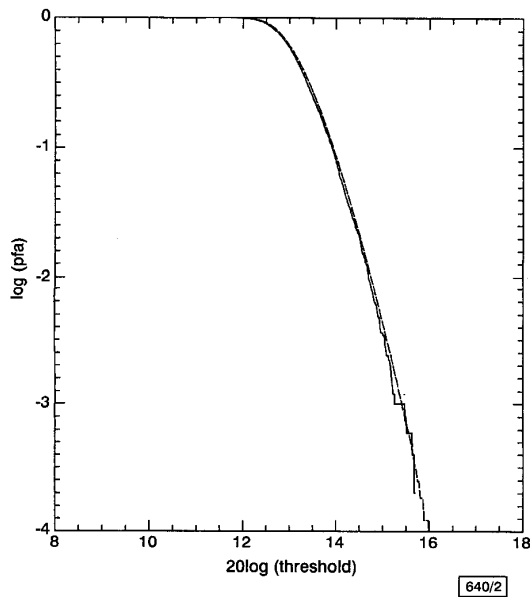


Fig. 2 Comparison of analytical result and numerical simulation for two-dimensional image

— numerical simulation
 - - - analytical result

Numerical simulation: The results given in the previous section were validated using numerical simulation.

Fig. 1 shows the comparison of eqn. 3 with the numerically derived false alarm curve for the envelope of a complex Gaussian process with a lowpass spectrum. Fig. 2 shows a comparison of the two-dimensional result contrasted with a simulation based on arrays of 512×512 complex Gaussian samples with a two-dimensional lowpass spectrum, again thresholding on the envelope. In each case excellent agreement is obtained between the analytical and theoretical results.

Conclusion: The false alarm curve for the envelope of a Gaussian random field is derived using a simple model; the curve has a simple analytical form and is insensitive to the details of the correlation function of the random field. Excellent agreement is obtained when the analytical results are compared with simulation for both

time series and two-dimensional images. The predictions of our analysis are borne out sufficiently by numerical simulation for it to be potentially useful in the analysis of the performance of matched filter detectors.

Acknowledgments: The authors wish to thank MOD for sponsoring this work.

© British Crown Copyright 2001
 Reproduced by permission of the Controller
 of Her Majesty's Stationery Office

1 December 2000

Electronics Letters Online No: 20010164
 DOI: 10.1049/el:20010164

R.D. Hill (DERA, St Andrews Road, Great Malvern, Worcs WR14 3PS, United Kingdom)

E-mail: rdhill@dera.gov.uk

R.J.A. Tough and K.D. Ward (TW Research, Harcourt Barn, Harcourt Road, Malvern, Worcs WR14 3DW, United Kingdom)

References

- WOODWARD, P.M.: 'Information theory and the design of radar receivers', *Proc. IRE*, 1951, **39**, pp. 1521-1524
- HILL, R.D., TOUGH, R.J.A., and WARD, K.D.: 'Distribution of the global maximum of a Gaussian random field and performance of matched filter detectors', *IEE Proc., Vis. Image Signal Process.*, 2000, **147**, (4), pp. 297-303
- RICE, S.O.: 'The mathematical analysis of random noise', *Bell Syst. Tech. J.*, 1944, **23**, pp. 282-332
- RICE, S.O.: 'The mathematical analysis of random noise', *Bell Syst. Tech. J.*, 1945, **24**, pp. 46-156
- WORSLEY, K.J.: 'Local maxima and the expected Euler characteristic of excursion sets of χ^2 , F and t fields', *Adv. Appl. Probab.*, 1994, **26**, pp. 13-42

Fast algorithm for over-complete wavelets

N.F. Law and W.C. Siu

The computational complexity of the over-complete wavelet representation is studied. It is found that the inverse transform is nearly three times more costly in computation than the forward transform. By exploiting the redundancy between the lowpass and the bandpass outputs, the computation is greatly simplified, resulting in an efficient inverse.

Introduction: The sub-sampling wavelet scheme provides a non-redundant multiresolution signal representation. However, this scheme is not translation invariant due to the sub-sampling operation. To achieve translation invariance, Mallat and Zhong proposed an alternative representation called the over-complete wavelet representation (OCWR) [1]. For the commonly used Spline family wavelet, this representation produces coefficients that correspond to multiscale edges in a signal. As points of sharp variations are important features for analysing signal properties [2], the OCWR provides a meaningful signal characterisation.

Despite its potential advantages, the OCWR has not received as wide an attention as the sub-sampling representation. One reason is that its computational complexity is much higher than that of the sub-sampling scheme [1, 3]. In this Letter, we study the computational complexity of the OCWR. By deriving a general expression for the complexity, it is found that the inverse is nearly three times more complicated than that of the forward transform. This is undesirable, especially for image compression. While the encoder can be very complicated, the decoder must be simple. To resolve the problem, the correlation between the lowpass and the bandpass outputs is studied. By exploiting this correlation inherent in the redundant OCWR, the computations are greatly simplified, thus resulting in an efficient inverse structure.

1D OCWR: The lowpass and the bandpass outputs are obtained through convolutions as follows:

$$X_1(z) = H(z)X_0(z) \quad (1)$$

$$D_1(z) = G(z)X_0(z) \quad (2)$$

where $X_0(z)$ is the original signal; and $H(z)$ and $G(z)$ denote, respectively, the lowpass and the bandpass filters. For a Spline wavelet with an arbitrary order n :

$$H(z) = \frac{z^n}{2^{2n+1}}(1+z^{-1})^{2n+1} \quad (3)$$

$$G(z) = 2(z^{-1} - 1) \quad (4)$$

In reconstruction:

$$X_0(z) = K(z)D_1(z) + \bar{H}(z)X_1(z) \quad (5)$$

where $\bar{H}(z)$ is the time inverse of $H(z)$, and $K(z)$ is the reconstruction filter which is written as

$$K(z) = \frac{1 - |H(z)|^2}{G(z)} \quad (6)$$

To analyse the computational complexity, the number of additions and multiplications are calculated. This complexity metric is of interest for both hardware and software realisations. The filters in eqns. 3 and 4 are firstly expanded by using eqn. 6 and the Binomial theorem as follows:

$$H(z) = \frac{1}{2^{2n+1}} \sum_{k=0}^n 2^{n+1} C_k [z^{n-k} + z^{-n+k-1}] \quad (7)$$

and

$$K(z) = B_{2n}(z^{2n+1} - z^{-2n}) + \sum_{k=1}^{2n} E_k [z^k - z^{-k+1}] \quad (8)$$

where

$$m C_r = \frac{m!}{r!(m-r)!}$$

$$B_m = \frac{1}{8} \sum_{k=m}^{2n} \frac{1}{2^{2k}} 2^k C_{k-m}$$

and $E_i = B_{i-1} - B_i$ (9)

The complexities of the filters defined in eqns. 4, 7 and 8 can be calculated for any arbitrary order n as follows:

$$\begin{aligned} \text{Complexity}(G) &= \text{Cost}_{add} + \text{Cost}_{multiply} \\ \text{Complexity}(H) &= \text{Complexity}(\bar{H}) \\ &= (2n+1)\text{Cost}_{add} + (n+1)\text{Cost}_{multiply} \\ \text{Complexity}(K) &= (4n+1)\text{Cost}_{add} + (2n+1)\text{Cost}_{multiply} \end{aligned} \quad (10)$$

where Cost_{add} and $\text{Cost}_{multiply}$ define the cost for an addition and a multiplication operation, respectively.

Theorem (i): The complexities of the forward and the inverse transforms using the filtering approach can be written as

$$\begin{aligned} \text{Complexity}_{FB}(\text{Forward}) &= (2n+2)\text{Cost}_{add} \\ &\quad + (n+2)\text{Cost}_{multiply} \\ \text{Complexity}_{FB}(\text{Inverse}) &= (6n+2)\text{Cost}_{add} \\ &\quad + (3n+2)\text{Cost}_{multiply} \end{aligned}$$

Proof of Theorem (i): The forward transform consists of filtering the input signal with $G(z)$ and $H(z)$. Thus the complexity of the forward transform is calculated by summing up $\text{Complexity}(G)$ and $\text{Complexity}(H)$. Similarly, the complexity of the inverse transform equals the sum of $\text{Complexity}(\bar{H})$ and $\text{Complexity}(K)$. \square

As can be seen from Theorem (i), the inverse transform has a significantly higher complexity (nearly three times) than the forward transform. This is undesirable and the computational complexity of the inverse transform has to be reduced.

Proposed spatial implementation: The OCWR provides a redundant signal representation. There exists a correlation between the lowpass and the bandpass outputs which can be exploited in our calculation of the wavelet transform. First, from eqns. 2 and 4, it can be shown that two recursion formulae can be formed as follows:

$$\begin{aligned} z^m X_0(z) &= X_0(z) - \frac{1}{2} D_1(z) \sum_{k=1}^m z^k \\ z^{-m} X_0(z) &= X_0(z) + \frac{1}{2} D_1(z) \sum_{k=1}^{m-1} z^{-k} \end{aligned} \quad (11)$$

By substituting eqns. 7 and 11 into eqn. 1 and using the fact that

$$2^{2n} = \sum_{k=0}^n 2^{n+1} C_k$$

we obtain the following equation:

$$\begin{aligned} X_1(z) &= X_0(z) + \frac{D_1(z)}{2^{2n+2}} \left\{ \sum_{l=0}^n 2^{n+1} C_{n-l} \sum_{k=0}^l z^{-k} \right. \\ &\quad \left. - \sum_{l=1}^n 2^{n+1} C_{n-l} \sum_{k=1}^l z^k \right\} \end{aligned} \quad (12)$$

Expanding the summations in eqn. 12 gives:

$$X_1(z) = X_0(z) + F[D_1(z)] \quad (13)$$

where

$$\begin{aligned} F[D_1(z)] &= \frac{D_1(z)}{2^{2n+2}} \left\{ 2^{2n} + \sum_{k=1}^n A_{n-k} (z^{-k} - z^k) \right\} \\ A_k &= \sum_{m=0}^k 2^{n+1} C_m \end{aligned} \quad (14)$$

Eqn. 13 shows that $X_1(z)$ can be obtained from not only $X_0(z)$ but also $D_1(z)$. This pure spatial relationship provides an alternative way for calculating the inverse wavelet transform. We can simply replace the addition with subtraction to reconstruct the signal. The new structure is shown in Fig. 1 for both the forward and the inverse transforms.

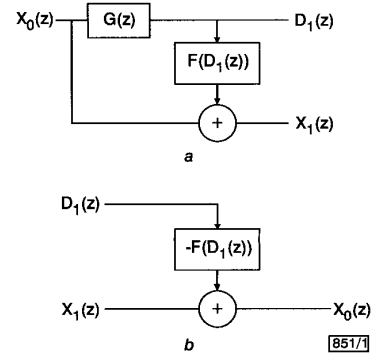


Fig. 1 New spatial domain 1D over-complete wavelet transform

a Forward
b Inverse

In analysing the complexity of the proposed spatial implementation, first note that the number of additions in $F[D_1(z)]$ is $2n$ and the number of multiplications is $n+1$.

Theorem (ii): The complexities of the 1D forward and inverse transforms of the proposed spatial algorithm are

$$\begin{aligned} \text{Complexity}_S(\text{Forward}) &= (2n+2)\text{Cost}_{add} \\ &\quad + (n+2)\text{Cost}_{multiply} \\ \text{Complexity}_S(\text{Inverse}) &= (2n+1)\text{Cost}_{add} \\ &\quad + (n+1)\text{Cost}_{multiply} \end{aligned}$$

Proof of Theorem (ii): The forward complexity equals the sum of the complexity of $G(z)$, the complexity of $F[D_1(z)]$, and one addition as shown in eqn. 13. The inverse complexity equals the sum of the complexity of $F[D_1(z)]$ and one addition. \square

Analysis: The complexity of the forward transform is lower than that of the inverse transform in the filter bank approach (Theorem (i)). In contrast, the complexity of the forward transform is slightly higher than that of the inverse transform in the new

approach (Theorem (ii)). By comparing the filter bank approach and the new approach, we can see that while the complexity of the forward transform remains the same, the complexity of the inverse transform shows a big difference. In the new approach, no filtering is required for the reconstruction of the original signal. Rather, a simple spatial implementation is used for the reconstruction and the computational complexity of the inverse transform is greatly reduced. Fig. 2 compares the computational complexity between the filter bank approach and the new spatial approach for different order n . The saving in computation is significant. For the quadratic spline ($n = 1$), the number of additions is reduced from 8 to 3 whereas the number of multiplications is reduced from 5 to 2. For the cubic spline ($n = 2$), the number of additions decreases from 14 to 5 whereas the number of multiplications decreases from 8 to 3.

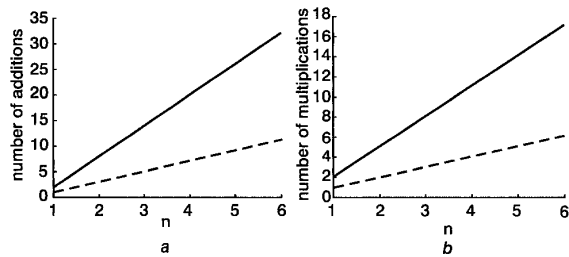


Fig. 2 Plots of number of additions and number of multiplications for different orders

a Additions
b Multiplications
— filter bank approach
- - - - - new approach

Conclusions: By deriving a general expression for the computational complexity of the over-complete wavelet representation, it is found that the inverse transform is nearly three times more complicated than the forward transform. To reduce the complexity, a new spatial implementation which exploits the correlation between the lowpass and the bandpass outputs is proposed. It is shown that the new implementation can greatly simplify the computations involved, thus resulting in an efficient inverse transform.

© IEE 2001
Electronics Letters Online No: 20010183
DOI: 10.1049/el:20010183

N.F. Law and W.C. Siu (Centre for Multimedia Signal Processing, Department of Electronic and Information Engineering, The Hong Kong Polytechnic University, Hung Hom, Hong Kong)

References

- MALLAT, S., and ZHONG, S.: 'Characterization of signals from multiscale edges', *IEEE Trans. Pattern Anal. Mach. Intell.*, 1992, **14**, pp. 710-732
- MARR, D.: 'Representing visual information' in HANSON, A., and RISEMAN, E.M. (Eds.): 'Computer vision system' (Academic Press, New York, 1978), pp. 61-80
- LIEW, A.W.C., LAW, N.F., and NGUYEN, D.T.: 'Direct reconstruction method for wavelet transform extrema representation', *IEE Proc. Vis., Image Signal Process.*, 1997, **144**, pp. 193-198

Multiscale-combined seismic waveform inversion using orthogonal wavelet transform

Jian-Wei Ma, Ya-Ping Zhu and Hui-Zhu Yang

A method of multiscale-combined inversion (MCI) using the orthogonal wavelet transform is applied to an inverse seismic waveform based on the convolutional model. MCI is a promising method because of its low dependence on the initial model, convergence efficiency and robustness. Numerical results show the effectiveness and potential of the method.

Introduction: The theory of the wavelet transform (WT) has developed rapidly over recent years and has been applied successfully in many different fields [1-4]. Numerous papers on multiscale optimal inversion based on the wave equation model have been published [5-7]. These methods are all forms of multiscale-independent inversion (MII).

The central idea of multiscale inversion is based on decomposing a problem into scale sequences and solving the problem from one scale to another. At long scales there are fewer local minima and those that remain are further apart from each other. MII focuses in particular on the fact that the local minima at a coarser scale are far apart from each other, allowing one to find the global minimum efficiently at the coarser scale and then switch to using finer scales. However, it has not taken full advantage of the coherent relation between scales. An MCI method based on the orthogonal WT is proposed to exploit the coherent relation between scales. The inversion result derived from using the coarser scale is used to impose constraints for the following scales, not merely as a good initial guess for the next scale. Also, the inversion result can be re-directed for the optimisation of the significant coefficients. Using the WT, the computational burden and local minimum are significantly less due to the sparseness and spatial relativity of the significant coefficients. A new formulation of the scale-constrained least mean square (LMS) method is proposed as one realisation of MCI. This Letter is devoted to MCI with the emphasis on the convolution model using the orthogonal wavelet transform.

Constrained LMS of convolution model: (i) *Convolution model:* In its simplest form, the 1D convolution problem can be written as

$$p(t) = s(t) * r(t) \quad (1)$$

where $p(t)$ is the received valid seismic trace, $s(t)$ is the seismic wavelet, and $r(t)$ is the reflectivity function. It can be rewritten in matrix form as

$$\mathbf{p} = \mathbf{S}\mathbf{r} \quad (2)$$

(ii) *Constrained LMS:* Using the Lagrange multiplier λ , the inversion of the above problem can be treated using the technique of linear LMS constrained finite power:

$$J = (\mathbf{p} - \mathbf{S}\mathbf{r})^T(\mathbf{p} - \mathbf{S}\mathbf{r}) + \lambda(\mathbf{r}^T\mathbf{r} - k') \quad (3)$$

$$J_{min} \Rightarrow \mathbf{S}^T\mathbf{S}\mathbf{r} - \mathbf{S}^T\mathbf{p} + \lambda\mathbf{r} = 0 \quad (4)$$

The stability of the inverse process can be improved by adding direct current λ to the entire systems.

MCI method based on convolution model: We transform the convolution model into the wavelet domain

$$\tilde{\mathbf{p}} = \tilde{\mathbf{S}}\tilde{\mathbf{r}} \quad (5)$$

where $\tilde{\mathbf{p}} = \mathbf{W}\mathbf{p}$, $\tilde{\mathbf{r}} = \mathbf{W}\mathbf{r}$ and $\tilde{\mathbf{S}} = \mathbf{W}\mathbf{S}\mathbf{W}^T$, respectively, correspond to the WT of the valid wave, the sequence of the reflection coefficients and the seismic wavelet. In this Letter, the decomposition by scale is applied to the source, to the observed data, and to the velocity model. The Daub4 wavelet [2] is adopted.

Combining the restriction of the finite power, the object function J can be rewritten as

$$J = (\tilde{\mathbf{p}} - \tilde{\mathbf{S}}\tilde{\mathbf{r}})^T(\tilde{\mathbf{p}} - \tilde{\mathbf{S}}\tilde{\mathbf{r}}) + \lambda(\tilde{\mathbf{r}}^T\tilde{\mathbf{r}} - k') + \gamma(\tilde{\mathbf{r}} - \tilde{\mathbf{r}}'_{jc})^T(\tilde{\mathbf{r}} - \tilde{\mathbf{r}}'_{jc}) \quad (6)$$

$$J_{min} \Rightarrow \tilde{\mathbf{S}}^T\tilde{\mathbf{S}}\tilde{\mathbf{r}} - \tilde{\mathbf{S}}^T\tilde{\mathbf{p}} + \lambda\tilde{\mathbf{r}} + \gamma(\tilde{\mathbf{r}} - \tilde{\mathbf{r}}'_{jc}) = 0 \quad (7)$$

where $\tilde{\mathbf{r}}'_{jc}$ denotes the inverse solution of the coarse scale, and $\tilde{\mathbf{I}}_{jc}$ is the part constrained identity operator. The Lagrange multipliers λ , γ restrict the diagonal elements in different ways. The general form constrained by several scales is shown in Fig. 1.

Numerical results and discussion: Fig. 2 shows a multi-layered velocity model that contains thin layers and lower-velocity layers. In this example, the spacial grid step size is 10m, the period of the seismic wavelet is 15ms, the minimal model velocity is 1800m/s, and the level number of multiscale decomposition is 7.

Fig. 2 clearly shows the evolving process of inversion from the coarser scale to the finer scale. It also shows the ability of MCI to pick up the thin layer. Since MCI devotes more attention to the